MASTER COPY

OAK RIDGE NATIONAL LABORATORY
operated by
UNION CARBIDE CORPORATION
for the
U.S. ATOMIC ENERGY COMMISSION

ORNL-TM-446

A TECHNIQUE FOR THE QUANTITATIVE CHARACTERIZATION OF DISPERSIONS

J. H. Cherubini
Sigfred Peterson

NOTICE

This document contains information of a preliminary nature and was prepared primarily for internal use at the Oak Ridge National Laboratory. It is subject to revision or correction and therefore does not represent a final report. The information is not to be abstracted, reprinted or otherwise given public dissemination without the approval of the ORNL patent branch, Legal and Information Control Department.

LEGAL NOTICE

This report was prepared as an account of Government sponsored work. Neither the United States, nor the Commission, nor any person acting on behalf of the Commission:

A. Makes any warranty or representation, expressed or implied, with respect to the accuracy, completeness, or usefulness of the information contained in this report, or that the use of any information, apparatus, method, or process disclosed in this report may not infringe privately owned rights; or

B. Assumes any liabilities with respect to the use of, or for damages resulting from the use of any information, apparatus, method, or process disclosed in this report.

As used in the above, "person acting on behalf of the Commission" includes any employee or contractor of the Commission, or employee of such contractor, to the extent that such employee or contractor of the Commission, or employee of such contractor prepares, disseminates, or provides access to, any information pursuant to his employment or contract with the Commission, or his employment with such contractor.

ORNL-TM-446

Copy

Contract No. W-7405-eng-26

METALS AND CERAMICS DIVISION

A TECHNIQUE FOR THE QUANTITATIVE CHARACTERIZATION OF DISPERSIONS

J. H. Cherubini and Sigfred Peterson

DATE ISSUED

FEB 18 1963

OAK RIDGE NATIONAL LABORATORY
Oak Ridge, Tennessee
operated by
UNION CARBIDE CORPORATION
for the
U. S. ATOMIC ENERGY COMMISSION

A TECHNIQUE FOR THE QUANTITATIVE CHARACTERIZATION OF DISPERSIONS

J. H. Cherubini[1] and Sigfred Peterson

ABSTRACT

Degradation of fuel particles encountered during the production of any metal matrix dispersion fuel is a recurring problem. During the development of dispersion fuel plates of UO_2 in stainless steel, it has been observed that changes in the fabrication process profoundly affect the quality of the dispersion. Two types of defects observed are fragmentation, in which the original particles are fractured and the ensuing fragments are distributed discretely in the matrix, and stringering, in which the original particles remain identifiable as an entity but are extended either plastically or by fracture. A method has been developed to quantitatively index the quality of dispersions, measuring the deviation due to both types of defects from a hypothetical ideal model in which the particles are represented by intact, randomly distributed spheres. The indexing method is demonstrated on a variety of dispersions of spherical UO_2 in stainless steel and found to reliably and reproducibly assess the quality of the dispersions.

INTRODUCTION

The fuel plates for the Core B of the Enrico Fermi Fast Breeder Reactor are roll-clad dispersions of 35 wt % −100 +140 mesh, spheroidal UO_2 dispersed in and clad with type 347 stainless steel.[2] The relatively large

[1]Presently with High Voltage Engineering, Quincy, Massachusetts.

[2]J. H. Cherubini, R. J. Beaver, and C. F. Leitten, Jr., Fabrication Development of UO_2-Stainless Steel Composite Fuel Plates for Core B of the Enrico Fermi Fast Breeder Reactor, ORNL-3077 (April 4, 1961).

UO_2 particle size and the spherical shape were selected according to the recommendations presented by Weir[3] in order to minimize irradiation damage of the fuel. In the course of fabrication development, it became increasingly obvious that both starting material and process changes profoundly affected the quality of the dispersion. It should be noted that the basic fabrication process involved hot rolling of pressed and sintered compacts of UO_2 dispersed in stainless steel. Naturally, the ideal product would be a dispersion of spherical particles randomly distributed in the stainless steel matrix. Deviations from ideality manifested themselves as stringering (extension of the particle in the rolling direction) and fragmentation (fracturing of the original particle and discrete distribution of the pieces in the matrix).

To compare the quality of various dispersions with an ideal dispersion, i.e., one in which spherical particles are unaffected by the fabrication process and are randomly distributed in the matrix, both an ideal model and a model which incorporated stringered and fragmented particles were constructed. Parameters were then established relating to the extent of fragmentation and stringering and allowing the comparison of different dispersions with each other and with the ideal dispersion. The indexing method has also been applied to dispersions of originally equiaxed, angular particles.

DERIVATION OF THE DISPERSION QUALITY INDICES

The effect of rolling on the geometry of dispersed particles is best considered in a plane section perpendicular to the plane of rolling and parallel to the rolling direction. To simplify the mathematical description of the dispersion, the dispersed particles may be grouped into three types, schematically illustrated in Fig. 1. Type A particles are spherical and have not been altered by fabrication. Type B particles, representative of fragmentation, are discretely distributed fragments of a larger particle. Type C particles, representative of stringering, are elongated in the rolling direction but are still identifiable as single particles.

---

[3]J. R. Weir, A Failure Analysis for the Low-Temperature Performance of Dispersion Fuel Elements, ORNL-2902 (May 27, 1960).

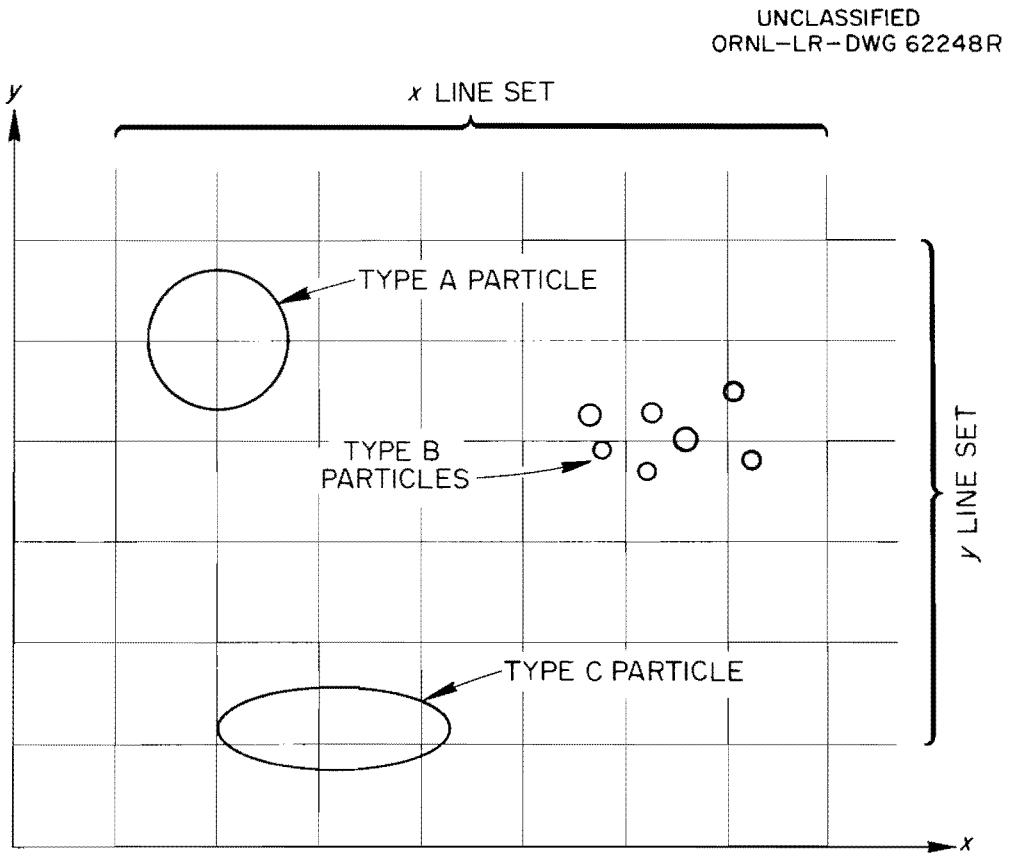

Fig. 1. Representative Model Particles in a Section of a Dispersion with Superimposed Grid Lines.

Consider a set of Cartesian coordinates in the plane of the section, with the x axis in the rolling direction. The different types of particles can be distinguished by the probability per unit length that random lines perpendicular to the axes intersect the particles. For the undamaged spherical type A particle, the probability of intersection is the same with lines perpendicular to either axis. The sum of the probabilities of intersection with the set of type B particles arising from a single original particle is greater than the probability of intersection with a type A particle of the same volume. The probability of intersection with the stringered type C particle depends obviously on direction, being greater for lines perpendicular to the x axis than for lines perpendicular to the y axis. On the basis of these considerations it is possible to derive quantitative indices measuring the degree of deviation of a given dispersion from the ideal defect-free dispersion.

To analyze a dispersion fuel, two sets of parallel lines are drawn, as shown in Fig. 1 on a photomicrograph of a section of the dispersion taken as described above. The lines of the x set are drawn perpendicular to the rolling direction (x axis) and the lines of the y set are parallel to the rolling direction. The number of particles intersected by each line set is determined and designated as x for the x set or y for the y set. Since it is the probability of intersection per unit length that is related to particle geometry, the numbers of intersections per unit length are calculated:

$$\bar{x} = \frac{x}{L_x} , \quad \bar{y} = \frac{y}{L_y}$$

where L_x and L_y are the total lengths of the lines in the sets.

The intersection densities $\bar{x}$ and $\bar{y}$, no matter what the particle geometry, will be greater the greater the concentration of the dispersion. Therefore, in order to compare different dispersions or even, because of some inevitable inhomogeneity, different parts of the same dispersion, it is necessary to adjust the intersection densities by dividing by the volume fraction α of the dispersed phase:

$$\bar{x}_v = \frac{\bar{x}}{\alpha} , \quad \bar{y}_v = \frac{\bar{y}}{\alpha} .$$

The adjusted intersection densities $\bar{x}_v$ and $\bar{y}_v$ can be related to the extent of fragmentation and stringering in the dispersion.

The volume fraction is readily determined from the photomicrograph since it is well-known that the volume fraction in a uniform dispersion is equal to the average area fraction of the dispersion in a plane section. Again, a grid of lines perpendicular to the axis is superimposed on the section (Fig. 1). The volume fraction α is simply the ratio of the number T_i of intersections between lines of the grid that coincide with particles to the total number T of grid intersections:

$$\alpha = \frac{T_i}{T} \quad .$$

The adjusted intersection densities $\bar{x}_v$ and $\bar{y}_v$ differ only due to stringering,with the intersection density being greater for the lines perpendicular to the x direction. Therefore, the stringering index S may be taken as the difference between the two adjusted densities:

$$S = \bar{x}_v - \bar{y}_v \quad .$$

A suitable fragmentation index is not as easily obtained. Since fragmentation increases the intersection densities, an index to measure fragmentation must depend on a comparison with an ideal unfragmented model. We may define an ideal index I as the intersection density of straight lines with randomly distributed spherical particles. The number of particles per unit volume of such a dispersion is clearly

$$N = \frac{\alpha}{(4/3)\pi R^3}$$

where R is the average particle radius. Since a line through the medium will intersect all particles with centers in a cylinder of radius R and cross-section area of πR^2 about the line, the number of intersections per unit length is

$$I = \pi R^2 N = \frac{3\alpha}{4R} \quad .$$

For comparing with intersection densities measured in a photomicrograph rather than in the actual scale of the specimen, the radius R should be

the actual particle radius multiplied by the magnification. The overall index ID, which measures the deviation from ideal, is then given by

$$ID = \bar{y} - I \quad .$$

Note that $\bar{y}$ rather than $\bar{y}_v$ is used, since I is intersections per unit length, not adjusted for dispersion concentration. The intersection density $\bar{y}$ is used, rather than $\bar{x}$, since its dependence on stringering is smaller and in the opposite direction to fragmentation.

The ideal index, of course, does not give a measure of fragmentation divorced from stringering. Stringering, we have already seen, affects the intersection densities $\bar{y}$ and $\bar{x}$. In addition, the phenomena of stringering and fragmentation can not really be separated. The same stresses produce both, and the fragments from one particle are generally aligned in the rolling direction and often in such close contact that it is difficult to differentiate between a collection of fragments and a stringered particle. Where considerable fragmentation occurs, a high degree of stringering is also observed.

Since fragmentation is accompanied by a high degree of stringering in dispersions made from spherical UO_2 in stainless steel, the overall index is generally negative. For a given stringering index, increasing degrees of fragmentation give smaller magnitudes of the overall index. A zero overall index results only if the dispersion is ideal – that is, free of both types of defects. In a near-ideal dispersion among the examples that follow, the small positive index noted reflects experimental error either in the indexing or in the particle radius used to calculate the ideal index. A significant positive index indicates a high degree of fragmentation without comparable stringering. This is observed in dispersions of angular fused and ground UO_2, but not in the dispersions of spherical UO_2 for which this indexing procedure was derived.

Since fragmented particles are generally aligned in the rolling direction, the magnitudes of the intersection density $\bar{y}$ and the indices calculated from it are sensitive to whether the grid lines coincide with these stringers. Thus considerable error can result if too coarse a grid

is used. This error may be minimized by adapting the automated technique developed by Moore and Wyman[4] in which a photomicrograph is scanned by a computer programmed to calculate density functions for the areas of different color or intensity.

INDEX DETERMINATION PROCEDURE

The procedure outlined below was found adequate for rapid indexing of the dispersions of interest. A useful form for recording the necessary information is reproduced in Appendix I.

I. Sample location

Select a 100X 5 in. × 7 in. photomicrograph of an area typical of the dispersion in question.

II. Area fraction determination

A. Superimpose on the photomicrograph a transparent film on which is scribed a 3/16-in.-square grid.

B. Count and record the number of grid intersections coinciding with UO_2 particles.

C. Calculate the area fraction α.

III. Determination of $\bar{x}_v$

A. Superimpose on the photograph a transparent film on which an x-line set is scribed (12 lines, $4\frac{1}{2}$ in. long, spaced at $\frac{1}{2}$-in. intervals).

B. Count and record the number of intersections of each line with dispersion particles.

C. Calculate $\bar{x}$ and $\bar{x}_v$.

IV. Determination of $\bar{y}_v$

Repeat III except use y-line set (9 lines, 6 in. long, spaced at $\frac{1}{2}$-in. intervals).

V. Calculate the ideal index.

VI. Calculate the stringering index and the overall index.

---

[4]G. A. Moore, L. L. Wyman, and H. M. Joseph, "Comments on the Possibilities of Performing Quantitative Metallographic Analysis with a Digital Computer," chapter from Quantitative Metallography, edited by F. N. Rhines, McGraw-Hill Co., Inc., New York (in press).

For reference, reproductions of the data sheets used in some of the following examples are included in Appendix II. It should be noted that fabricability indices calculated from photomicrographs of different magnifications cannot be directly compared without appropriate correction. For example, a 50X photomicrograph of a given specimen contains four times the area, hence four times the number of particles, as a 100X view of the same specimen at the same print size.

The precision and accuracy of the above procedure can be improved by decreasing the photomicrograph magnification for a given size print, increasing the number of lines in the x- and y-line sets, or decreasing the square size of the grid used in the area percent determination.

APPLICATION OF DISPERSION INDEXING

In the course of developing manufacturing techniques for the Fermi Core B fuel plates, considerable variations in dispersion quality were noted between lots of commercial spheroidal UO_2 with the fabrication techniques fixed. For example, sections of samples F-128A and F-131A, which were fabricated according to established procedures[5] and differ only in the lot of UO_2 dispersed, are shown in Figs. 2 and 3, respectively. The fuel sections are dispersions of 35 wt % −100 +140 mesh spheroidal UO_2 in type 347 stainless steel, which have been hot reduced 87% in thickness at 1200°C and finished by cold rolling 3.5%. The structure of F-131A is qualitatively judged superior to that of F-128A for it appears more like the ideal model. The observations are substantiated upon comparing the stringering and overall indices for these specimens in Table 1. The stringering index of F-131A is less than one half that of F-128A, quantitatively verifying the improvement in dispersion quality. Since specimen F-128A has a smaller negative overall index than F-131A despite a greater stringering index, it can be inferred that F-128A is characterized by significantly more fragmentation as well as stringering. It should be recognized that stringering algebraicly reduces the overall index while fragmentation increases it.

---

[5] J. H. Cherubini, R. J. Beaver, and C. F. Leitten, Jr., Fabrication Development of UO_2-Stainless Steel Composite Fuel Plates for Core B of the Enrico Fermi Fast Breeder Reactor, ORNL-3077 (April 4, 1961).

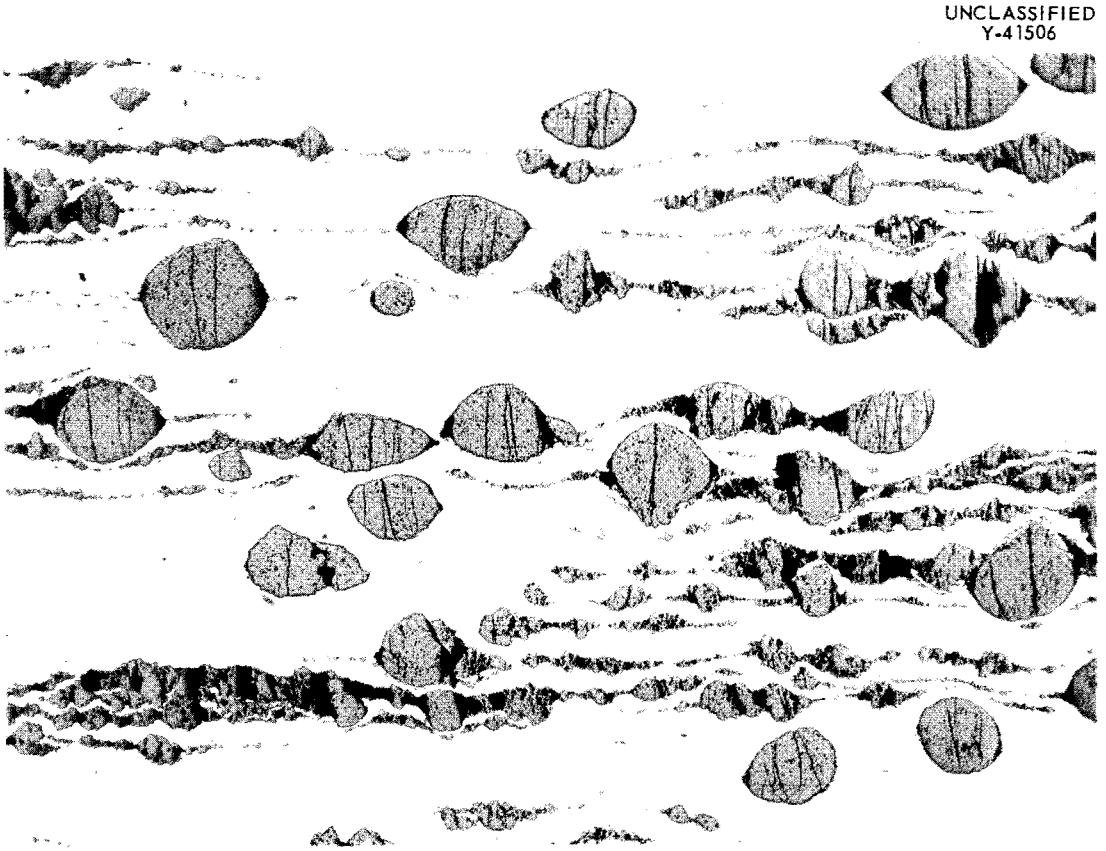

Fig. 2. Sample F-128A Containing 35 wt % −100 +140 Mesh Spheroidal UO_2 (Batch J-01-EN) Dispersed in Type 347 Stainless Steel; 3.5% Cold Rolled After 87% Hot Reduction in Thickness. 100X. As-polished.

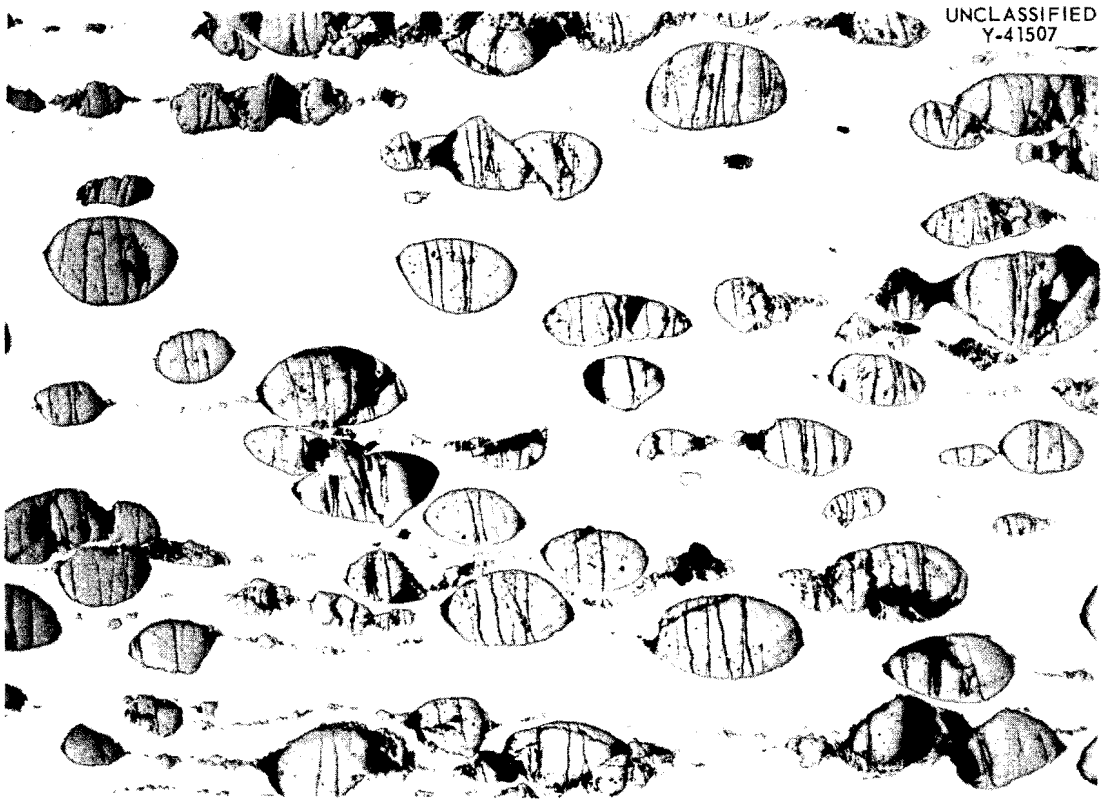

Fig. 3. Sample F-131A Containing 35 wt % −100 +140 Mesh Spheroidal UO_2 (Batch J-07-EN) Dispersed in Type 347 Stainless Steel; 3.5% Cold Rolled After 87% Hot Reduction in Thickness. 100X. As-polished.

Table 1. Quality Index Determination of Several Dispersion Fuels

Fuel Plate	Volume Fraction UO_2 (α)	Intersection Density (in.$^{-1}$)		Adjusted Intersection Density (in.$^{-1}$)		Ideal Index (in.$^{-1}$) I	Stringering Index (in.$^{-1}$) S	Overall Index (in.$^{-1}$) ID
		$\bar{x}$	$\bar{y}$	$\bar{x}_v$	$\bar{y}_v$			
F-128A	0.336	3.44	0.80	10.25	2.37	0.97	7.9	−0.17
F-128A[a]	0.336	3.32	0.78	9.86	2.31	0.97	7.6	−0.19
F-131A	0.395	2.24	0.87	5.68	2.20	1.14	3.5	−0.27
F-169A	0.356	3.22	0.76	9.05	2.13	1.08	6.9	−0.32
F-282	0.240	0.98	0.81	4.10	3.38	0.73	0.7	+0.08
F-262	0.222	3.28	1.53	14.80	7.79	0.73	7.0	+0.80

[a]Second analysis of sample by a different operator.

In order to determine whether or not the indexing process is operator independent, the fabricability indices of the F-128A sample were determined by a second operator. A comparison of the fabricability index determinations by the two operators is also shown in Table 1. As can be seen, the $\bar{y}_v$ values differ by only 2.6%, the $\bar{x}_v$ values by only 4%, showing that the method is reasonably free from human error.

Sample F-169A was fabricated completely independently of sample F-128A, but using the same materials and procedure. Table 1 shows these samples have a comparable stringering index and a not greatly different overall index. It is difficult to judge this by mere visual comparison of the structures shown in Figs. 2 and 4. However, the indexing procedure shows that the microstructures of the two samples are similar. The ability to compare such supposedly identical dispersions suggests that, within limits, the indexing procedure is a useful quality control tool.

Sample F-282 illustrated in Fig. 5 is a dispersion of particularly high quality that contains nominally 30 wt % −100 +140 mesh UO_2 in type 347 stainless steel, fabricated identically with the preceding examples except that the cold-rolling operation was omitted. The fabricability indices of this dispersion are also included in Table 1.

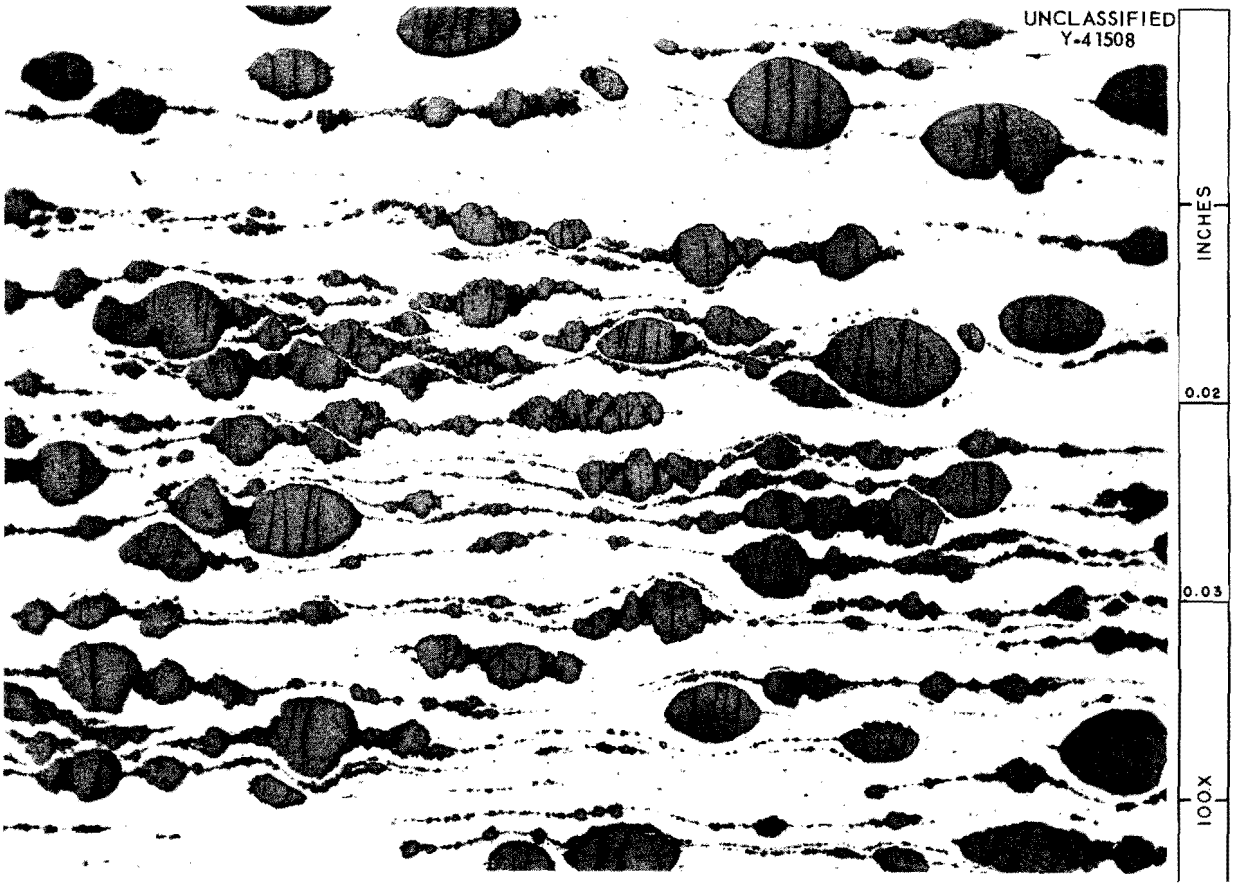

Fig. 4. Sample F-169A Containing 35 wt % −100 +140 Mesh Spheroidal UO_2 (Batch J-01-EN) Dispersed in Type 347 Stainless Steel; 3.5% Cold Rolled After 87% Hot Reduction in Thickness. 100X. As-polished.

Fig. 5. Sample F-282 Containing 30 wt % −100 +140 Mesh Spheroidal UO_2 (Batch H-03-HA) Dispersed in Type 347 Stainless Steel. As-hot-rolled. Etchant: Glyceria regia. 100X.

Its low stringering index 0.72 is close to ideal (zero). Here again, the original batch of UO_2 is different from that used in the other two similar dispersions and the superior quality of the dispersion can be attributed to the high bulk density of the UO_2 spheroids. Final cold rolling as used in the previous examples has little effect on the dispersion quality.[6] The majority of the stringering is due to plastic flow of the UO_2 rather than particle fracture and subsequent stringering. The low stringering index, coupled with the low overall index of 0.08 (ideally also zero), demonstrates that sample F-282 is close to ideal.

The analysis has been extended to nonspherical particles. Sample F-262, shown in Fig. 6 is a 35 wt % dispersion in type 347 stainless steel of −100 +140 mesh fused and ground UO_2 particles of an equiaxed, angular shape, fabricated identically to the preceding "ideal" dispersion (Fig. 6). Obviously, the particles have failed to maintain their original integrity, and pieces of what had been one large particle are discretely dispersed throughout the matrix. Very little particle stringering of the type illustrated in the preceding examples has occurred; however, the major axis of virtually every particle is parallel to the rolling direction. These visual observations are supported by the indices reported in Table 1. The stringering index is 7.01 (due in part to reorientations of unsymmetrical particles); the overall index is +0.80. This points out that the physical nature of the system under examination must be considered and the associated indices, per se, cannot be considered wholly descriptive of the sample in question. It is interesting to note that the high positive overall index, despite a high stringering index, indicates an extremely large amount of fragmentation.

Figure 7a and 7b represent two sections taken from a single as-hot-rolled fuel plate containing 25 wt % −170 +325 mesh spheroidal UO_2 dispersed in type 430 stainless steel. The fabricability indices of both are listed in Table 2. In both sections, the stringering index S and the overall fabricability index ID are essentially the same, demonstrating that the quality of the dispersion did not vary unreasonably in the fuel plate.

The dispersion shown in Fig. 7c is a sample prepared by the same UO_2 loading and fabrication procedure as the preceding but containing −100 +325

---

[6] Ibid.

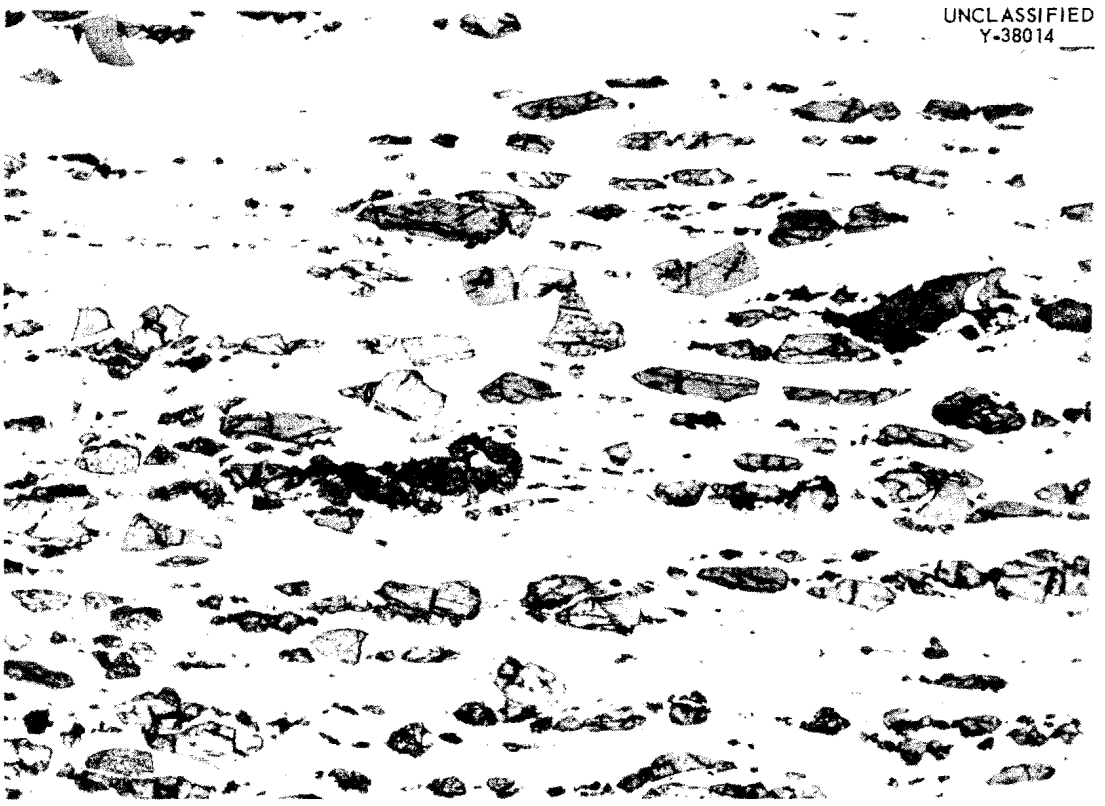

Fig. 6. Sample from Plate F-262 Containing 35 wt % −100 +140 Mesh Fused and Ground UO_2 Dispersed in Type 347 Stainless Steel. Fabrication route identical to plate F-282. 100X. As-polished.

(a)

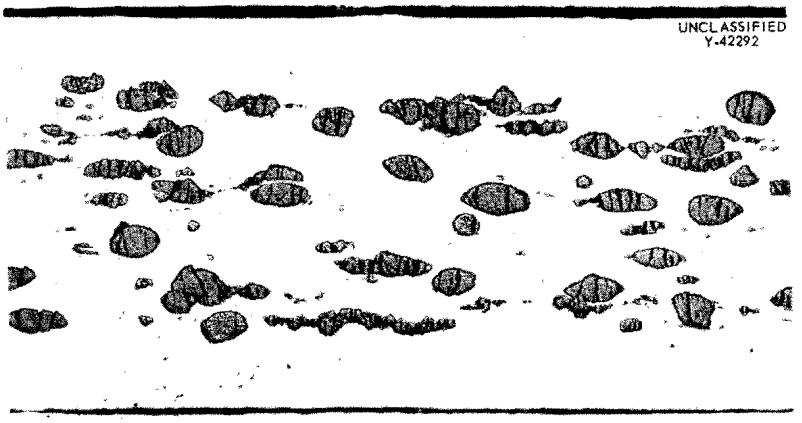

(b)

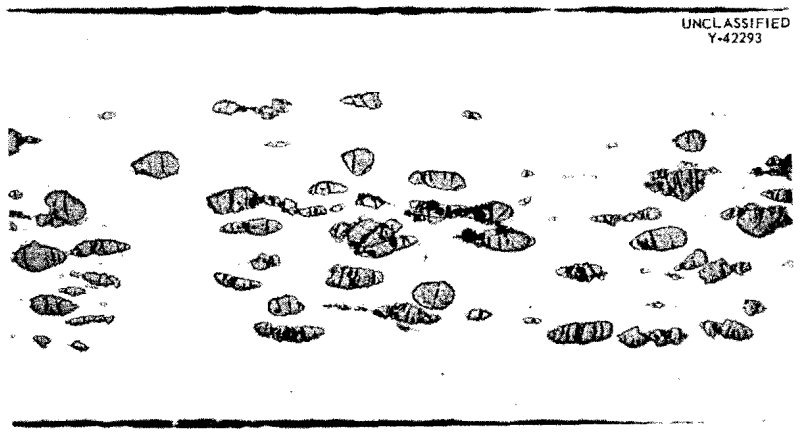

(c)

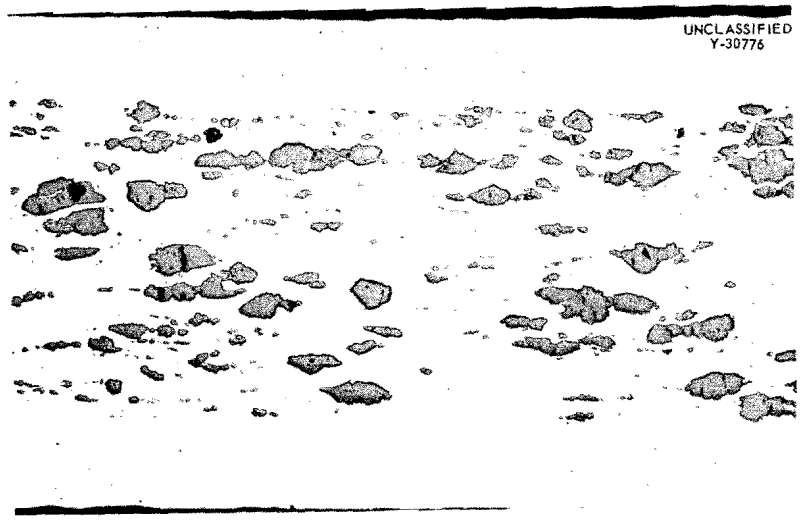

Fig. 7. (a) 25 wt % −170 +325 Mesh Spheroidal UO_2 (Batch A-536) Dispersed in Type 430 Stainless Steel. As-hot-rolled. Location 1. As-polished. 100X. (b) Same as (a) but at Location 2. As-polished. 100X. (c) Same as (a) but contains −100 +325 mesh hydrothermal UO_2. As-polished. 100X. Reduced 28%.

Table 2. Effect of Sample Location and UO_2 Type on the Fabricability Index of As-Hot-Rolled Dispersion Fuel Sections

UO_2 Type	UO_2 Cut (mesh)	$\bar{x}$	$\bar{y}$	α	$\bar{x}_v$	$\bar{y}_v$	I	S	ID
		(in.$^{-1}$)							
Spheroidal[a]	−170 +325	2.295	0.968	0.261	8.79	3.71	1.88	5.08	−0.91
Spheroidal[a]	−170 +325	1.920	0.875	0.226	8.50	3.87	1.69	4.63	−0.81
Hydrothermal	−100 +325	2.71	1.425	0.216	12.50	6.60	1.25	5.90	+0.18

[a]Specimens taken from two different locations in the same dispersion plate.

mesh angular UO_2 produced by the hydrothermal process. This sample has a stringering index about the same as the preceding examples although it arises from both stringering and particle reorientation. The high $\bar{y}_v$ value can be interpreted as due to either a finer mean particle size or more fragmentation during processing. These two effects cannot be unambiguously separated, for the ideal index is sensitive to small errors in the mean radius of particles as small as these and hence is subject to considerable error. Nevertheless, a semiquantitative assessment can be made. The ideal index of 1.25 in.$^{-1}$ in Table 2 is based on an original weighted average particle radius of R = 1.3 mils. The positive value of the overall index, coupled with the large stringering index, indicates that considerable particle fragmentation was experienced by the hydrothermally produced UO_2.

CONCLUSIONS AND SUMMARY

A quantitative method, enabling the assessment of dispersion quality by measuring the degradation of the dispersoid, is mathematically derived. In this method, the dispersion is compared to an ideal dispersion of randomly situated, integral, spherical particles. Fabricability indices reflecting both the extent of particle fragmentation and stringering can be computed which, together with a qualitative description, can reliably

classify a given dispersion. A rapid method of determination of these dispersion quality indices, subject to relatively small variation due to its application by different operators, is demonstrated.

On applying the method to several dispersions, spheroidal UO_2 was found to stringer to an extent depending on the particular lot although its propensity toward fragmentation was small. On the other hand, both fused and ground and hydrothermally produced oxide suffered considerable fragmentation.

ACKNOWLEDGMENT

The authors are indebted to C. F. Leitten, Jr., for a critical evaluation of the work, to the Metallography group for preparation of photomicrographs, to the Metals and Ceramics Division Reports Office for valuable assistance in producing this report, and to E. R. Turnbill for assistance in applying the method reported.

APPENDIX I

RECORD DATA SHEETS USED FOR DETERMINATION OF FABRICABILITY INDICES

I. Sample Description _____

_____

Photo number _____

Magnification _____

Equivalent sample area (square mils) _____

Particles or particle grouping in picture _____

II. Area Percent Determination _____

Grid description: Square size (in.) _____

Description _____

Number of particle intersections _____

Area fraction (α) _____

III. $\bar{x}_v$ Determination

Grid description: Number of lines _____

Length of lines each _____ total _____

Line spacing _____

Intersections per line

1	2	3	4	5	6	7	8	9	10	11	12

Intersections: Total _____

Av per in. ($\bar{x}$) _____

$\bar{x}_v = \frac{\bar{x}}{\alpha}$ _____

IV. $\bar{y}_v$ Determination

Grid description: Number of lines _____

Length of lines each _____ total _____

Line spacing _____

Intersections per line

1	2	3	4	5	6	7	8	9	10	11	12

Intersections: Total _____

Av per in. ($\bar{y}$) _____

$\bar{y}_v = \frac{\bar{y}}{\alpha}$ _____

V. Estimated Mean Particle Radius, $\bar{R}$, (mils) _____

Ideal index ($I = \frac{3}{4}\frac{\alpha}{\bar{R}}$) _____

VI. Stringering Index ($\bar{x}_v - \bar{y}_v$) = S _____

Overall index ($\bar{y} - I$) = ID _____

APPENDIX II

WORK SHEETS FOR EXAMPLES I AND II

I. Sample Description Example I, Operator I, Plate No. F-128A, Batch J-01-EN UO_2 Dispersed in type 347 stainless steel; 3.5% cold rolled

Photo number Y-41506

Magnification 100X

Equivalent sample area (square mils)

Particles or particle grouping in picture 73

II. Area Percent Determination

Grid description: Square size (in.) 3/16

Description 23 × 32 = 736 intersections

Number of particle intersections 247

Area fraction (α) 0.336

III. $\bar{x}_v$ Determination

Grid description: Number of lines 12

Length of lines each $4\frac{1}{2}$ in. total 54 in.

Line spacing $\frac{1}{2}$ in.

Intersections per line

1	2	3	4	5	6	7	8	9	10	11	12
16	18	17	21	15	16	11	12	12	14	17	17

Intersections: Total 186

Av per in. ($\bar{x}$) 3.44

$\bar{x}_v = \frac{\bar{x}}{\alpha}$ 10.25

IV. $\bar{y}_v$ Determination

Grid description: Number of lines 9

Length of lines each 6 in. total 54 in.

Line spacing $\frac{1}{2}$ in.

Intersections per line

1	2	3	4	5	6	7	8	9	10	11	12
2	6	7	5	5	4	6	3	5			

Intersections: Total 43

Av per in. ($\bar{y}$) 0.80 per in.

$\bar{y}_v = \frac{\bar{y}}{\alpha}$ 2.37

V. Estimated Mean Particle Radius, $\bar{R}$, (mils) 2.6 = 0.26 in. magnified

Ideal index ($I = \frac{3}{4}\frac{\alpha}{\bar{R}}$) 0.97 per in.

VI. Stringering Index ($\bar{x}_v - \bar{y}_v$) = S 7.9

Overall index ($\bar{y} - I$) = ID -0.17

I. Sample Description Example I, Operator 2; Plate No. F-128A, Batch J-01-EN UO_2 Dispersed in type 347 stainless steel; 3.5% cold rolled

Photo number Y-41506

Magnification 100X

Equivalent sample area (square mils) _____

Particles or particle grouping in picture 73

II. Area Percent Determination _____

Grid description: Square size (in.) 3/16

Description 23 × 32 = 736 intersections

Number of particle intersections 247

Area fraction (α) 0.336

III. $\bar{x}_v$ Determination

Grid description: Number of lines 12

Length of lines each $4\frac{1}{2}$ in. total 54 in.

Line spacing $\frac{1}{2}$ in.

Intersections per line

1	2	3	4	5	6	7	8	9	10	11	12
18	18	12	12	13	11	15	16	18	13	17	16

Intersections: Total 179

Av per in. ($\bar{x}$) 3.32

$\bar{x}_v = \frac{\bar{x}}{\alpha}$ 9.86

IV. $\bar{y}_v$ Determination

Grid description: Number of lines 9

Length of lines each 6 in. total 54 in.

Line spacing $\frac{1}{2}$ in.

Intersections per line

1	2	3	4	5	6	7	8	9	10	11	12
5	4	5	4	6	5	6	1	6			

Intersections: Total 42

Av per in. ($\bar{y}$) 0.78 per in.

$\bar{y}_v = \frac{\bar{y}}{\alpha}$ 2.31

V. Estimated Mean Particle Radius, $\bar{R}$, (mils) 2.6 = 0.26 in. magnified

Ideal index ($I = \frac{3}{4}\frac{\alpha}{\bar{R}}$) 0.97 per in.

VI. Stringering Index ($\bar{x}_v - \bar{y}_v$) = S 7.5

Overall index ($\bar{y} - I$) = ID −0.19

I. Sample Description Example II, Plate F-131A, Batch J-07-EN UO_2 Dispersed in type 347 stainless steel; 3.5% cold rolled

Photo number Y-41507

Magnification 100X

Equivalent sample area (square mils)

Particles or particle grouping in picture 72

II. Area Percent Determination

Grid description: Square size (in.) 3/16

Description 32 × 23 = 736 intersections

Number of particle intersections 291

Area fraction (α) 0.395

III. $\bar{x}_v$ Determination

Grid description: Number of lines 12

Length of lines each $4\frac{1}{2}$ in. total 54 in.

Line spacing $\frac{1}{2}$ in.

	1	2	3	4	5	6	7	8	9	10	11	12
Intersections per line	13	9	10	8	9	11	10	9	10	11	10	11

Intersections: Total 121

Av per in. ($\bar{x}$) 2.241

$\bar{x}_v = \frac{\bar{x}}{\alpha}$ 5.68

IV. $\bar{y}_v$ Determination

Grid description: Number of lines 9

Length of lines each 6 in. total 54 in.

Line spacing $\frac{1}{2}$ in.

	1	2	3	4	5	6	7	8	9	10	11	12
Intersections per line	5	2	8	4	4	7	3	8	6			

Intersections: Total 47

Av per in. ($\bar{y}$) 0.87

$\bar{y}_v = \frac{\bar{y}}{\alpha}$ 2.20

V. Estimated Mean Particle Radius, $\bar{R}$, (mils) 2.6 = 0.26 in. magnified

Ideal index ($I = \frac{3}{4}\frac{\alpha}{\bar{R}}$) 1.14

VI. Stringering Index ($\bar{x}_v - \bar{y}_v$) = S 3.38

Overall index ($\bar{y} - I$) = ID −0.27

INTERNAL DISTRIBUTION

1–2. Central Research Library
3–4. Document Reference Section
5–9. Laboratory Records
10. Laboratory Records, RC
11–25. Division of Technical Information Extension
26. Research and Development Division, ORO
27–28. Reactor Division, ORO
29. ORNL Patent Office
30. G. M. Adamson, Jr.
31. R. J. Beaver
32. E. S. Bomar
33. B. S. Borie
34. J. E. Cunningham
35. R. G. Donnelly
36. D. A. Douglas, Jr.
37. A. P. Fraas
38. J. H Frye, Jr.
39. J. P. Hammond
40. W. O. Harms
41. R. L. Heestand
42–44. M. R. Hill
45. D. O. Hobson
46. J. A. Lane
47–49. C. F. Leitten, Jr.
50. H. G. MacPherson
51. W. D. Manly
52. M. M. Martin
53. R. W. McClung
54. R. E. McDonald
55. C. J. McHargue
56. F. R. McQuilkin
57. P. Patriarca
58. S. Peterson
59. L. D. Schaffer
60. G. M. Slaughter
61. J. A. Swartout
62. A. J. Taylor
63–64. W. C. Thurber
65. D. B. Trauger
66. T. D. Watts
67. J. R. Weir
68. Bruce Anderson, AEC, COO
69. A. L. Benson, AEC, ORO
70. J. L. Gregg (consultant)
71. W. J. Larkin, AEC, ORO
72. J. A. Redeck, AEC, COO
73. D. K. Stevens, AEC, Washington
74. G. M. Wensch, AEC, Washington

EXTERNAL DISTRIBUTION

75. J. H. Cherubini, High Voltage Engineering, Quincy, Mass.
76. W. H. Jens, APDA
77–81. A. A. Shoudy, APDA
82. R. C. Williams, APDA